(Received 7 January 2026, Accepted 16 March 2026, Scheduled 5 April 2026)

Design and Experimental Validation of a Modified Compact 2×2 Orthogonal Microstrip MIMO Antenna for Sub-6 GHz 5G Systems

Hayder M. Mutashar and Mohammad S. Bayati*

Department of Electrical Engineering, Razi University, Kermanshah, Iran

ABSTRACT: This paper presents the design, optimization, fabrication, and experimental validation of a compact 2×2 microstrip Multiple-Input Multiple-Output (MIMO) antenna for 5G sub-6 GHz applications. The proposed antenna is centered at 5.5 GHz and implemented on an FR4 substrate with an overall size of $60 \times 60\,\text{mm}^2$, making it suitable for integration into modern compact wireless devices. The design process begins with the development of a single Planar Microstrip Monopole Antenna (PMMA), which is enhanced using a systematic stub-loading technique to improve impedance matching, radiation stability, and efficiency. The optimized element is then replicated and arranged using an orthogonal placement strategy to reduce mutual coupling without employing additional decoupling structures or parasitic components. The proposed MIMO configuration achieves excellent impedance matching, with a measured reflection coefficient of approximately -49 dB at 5.5 GHz and an operational bandwidth extending from 4.7 to 6.49 GHz. The antenna exhibits high radiation efficiency (≈ 81) and total efficiency (≈ 79) within the operating band. The measured peak gain reaches 4.70 dBi, showing close agreement with simulated results. Diversity performance is confirmed by an extremely low envelope correlation coefficient ($ECC < 0.0001$) and a diversity gain approaching 10 dB, indicating strong spatial diversity and reliable multipath performance. Furthermore, the Total Active Reflection Coefficient (TARC) remains below -10 dB across the main operating region, validating stable multi-port excitation behavior. The combination of compact size, high efficiency, excellent isolation, and low structural complexity demonstrates that the proposed antenna provides a practical and cost-effective solution for sub-6 GHz 5G MIMO systems.

1. INTRODUCTION

Recently, nearly everything connects without wires from homes to hospitals, factories to cars, and invisible signals carry information constantly [1]. More gadgets are now connected than ever before — phones, sensors, machines, and even entire cities [2]. Streaming video, self-driving vehicles, remote surgeries, and massive online networks push old systems to their limits. Speed matters more. Delays feel worse for users [3]. Connections must hold strong when they are needed most. Signals are packed tighter into airwaves, demanding smarter handling. Engineers respond by refining how antennas send and receive energy through space. Each upgrade helps squeeze better results from crowded frequencies in the wireless medium. Therefore, the evolution keeps moving because what worked yesterday falls short today [4].

One step at a time, wireless tech has moved forward, fixing old problems while adding fresh features. First, the First Generation (1G) and Second Generation (2G) handled only voice calls and short written messages, with almost no room for data. Then came the change to the Third Generation (3G), and later the Fourth Generation (4G) opened doors to fast internet on phones, video chats, and smooth download. Currently, the Fifth Generation (5G) takes another leap, powering super-sharp videos, digital worlds one can interact with, smart traffic networks, and devices talking to one another by the millions. Each shift built quietly on what was already there, growing smarter without shouting about it [5].

In the field of the recent 5G systems, the primary service categories are enhanced Mobile Broadband (eMBB), Ultra-Reliable Low-Latency Communications (URLLC), and massive Machine-Type Communications (mMTC). To meet these high-end requirements, new physical-layer technologies are being developed, which can improve the capacity of the channel, reduce multipath fading, and improve the overall performance of the link. Among these technologies, the Multiple-Input Multiple-Output (MIMO) technique is considered the most important. This technique can improve the overall data rate without the need for any increase in bandwidth or transmitting power [6].

In addition, microstrip antennas have emerged as one of the most viable candidates for sub-6 GHz 5G use cases owing to their low-profile configuration, lightweight design, and the ease of integrating them with the printed circuit board [7]. These characteristics make the microstrip antenna an attractive option for the design of compact wireless devices, such as smartphones, wearable electronics, Internet of Things (IoT) devices, and vehicular communication systems. Furthermore, the microstrip antenna is suitable for mass production, which is critical for the commercialization of the technology [8].

* Corresponding author: Mohammad S. Bayati (s.bayati@razi.ac.ir).

Although microstrip antennas offer a wide range of benefits, some of the inherent disadvantages of microstrip antennas are their relatively narrow bandwidth, moderate efficiency, surface waves, and strong mutual coupling between closely spaced antennas. The problem is further complicated in MIMO systems, as closely spaced antennas tend to show a strong correlation between each other, resulting in poor isolation between antennas [9].

In order to overcome the limitations, various enhancement techniques have been suggested in the literature. Radiator geometries [10], slots [11], parasitic elements [12], and fractals are some of the commonly used techniques for enhancing the bandwidth by controlling the surface current distribution [13]. Another powerful method for enhancing the bandwidth and efficiency without increasing the antenna size is the use of defected ground structures, which can effectively control the surface waves and provide an extended current path [14].

In compact MIMO systems, the reduction of mutual coupling between the antenna elements is a major challenge [15]. Conventional techniques to mitigate this problem involve the use of neutralization lines, electromagnetic bandgap structures, metasurfaces, and decoupling elements. Although these techniques are effective, they add complexity to the design process and the cost of the final structure. A simple technique to minimize the problem of mutual coupling involves the use of polarization diversity. In this technique, the elements of the antenna are placed at right angles to each other. As a result, the electromagnetic fields become orthogonal to each other [16].

In view of the stringent performance requirements of sub-6 GHz 5G communication systems and the inherent difficulties of compact microstrip MIMO integration, in this work, a compact and efficient 2×2 microstrip MIMO antenna design, fabrication, and experimental validation are presented. In the proposed design, a planar microstrip monopole antenna, a defected partial ground structure, and an orthogonal arrangement are integrated to improve the impedance matching, efficiency, isolation, and diversity performance without increasing the design complexity of the microstrip MIMO antenna.

An important contribution of the research is the realization of effective mutual coupling reduction through the application of geometric orthogonality instead of the need for decoupling networks, parasitic elements, metasurfaces, and multilayer structures. This is done while maintaining simplicity in the structure along with high electromagnetic performance within the compact $60 \times 60\,\text{mm}^2$ footprint. The antenna has good impedance matching around 5.5 GHz, high radiation and total efficiency, good gain performance, low envelope correlation coefficient ($ECC < 0.0001$), and high diversity gain close to the theoretical limit. As part of the extended sub-6 GHz 5G applications, the intended 5.5 GHz frequency is located inside the officially defined 5G NR-U (Band n46) spectrum (5150–5925 MHz) [17].

The proposed MIMO system comprises four identical planar radiating structures connected to a 50-Ω coaxial cable for balanced power distribution. Analytical dimension estimation, full-wave optimization, and fabrication are followed by thorough experimental validation. The performance of the proposed MIMO system is evaluated by analyzing the reflection coefficient, mutual coupling, efficiency, peak gain, radiation characteristics, Total Active Reflection Coefficient (TARC), diversity gain, and ECC to ascertain the reliability of the proposed MIMO system.

The entire paper, therefore, proves that it is possible to achieve high levels of isolation, diversity, and radiation efficiency in a compact microstrip MIMO antenna design without adding complexity to its structure, making the proposed antenna a viable and affordable option for current and future 5G wireless communication devices operating in the sub-6 GHz frequency band.

2. LITERATURE SURVEY

In recent years, substantial research activities have been focused on designing compact and high-performance MIMO antenna systems for 5G wireless communication systems operating below 6 GHz. Various techniques, including the optimization of radiator geometry, defected ground structures, polarization diversity techniques, metasurface technology, and dielectric resonator techniques, have been investigated by researchers to overcome the limitations of bandwidth, cross-talk issues, and low radiation efficiency associated with compact microstrip antennas used for MIMO systems. Various research works have been reported in the literature on this topic, some of which are discussed in this section.

In [18], Saeidi et al. propose a miniaturized dual-band MIMO antenna based on spiral-button radiator structures for sub-6 GHz 5G networks. A full ground plane is employed for reducing the effects of the body and Specific Absorption Rate (SAR). The proposed antenna ensures reliable dual-band operation, good impedance matching, and stable operation under body loading conditions.

In [19], Upadhyaya et al. proposed an aperture-fed quad-port dielectric resonator antenna MIMO system for sub-6 GHz 5G and WLAN applications. The proposed MIMO system uses a dielectric resonator antenna that provides a wide bandwidth and efficiency, as well as a strong inter-element isolation through aperture coupling. The proposed MIMO system shows a high efficiency rate as well as a stable radiation pattern within the operating range.

In [20], Ez-Zaki et al. proposed a MIMO antenna based on a Koch fractal structure along with the design of a double-negative metamaterial structure for sub-6 GHz vehicular communication. The metamaterial is designed to reduce the mutual coupling effect and surface waves. The results are validated through simulation and measurement.

Following that, in [21], Morsy proposes a compact eight-element MIMO antenna array for sub-6 GHz mobile terminals. The antenna array and feeding mechanism have been optimized to integrate a large number of elements in a small form factor. The results have been satisfactory, and the MIMO smartphone supports high-order MIMO system.

Furthermore, in [22], Hasan et al. examine a wideband sub-6 GHz MIMO antenna design enabled by a metasurface superstrate. The metasurface is introduced to improve the isolation and gain of the antenna. A significant improvement in isola-

tion and gain is achieved in a compact planar form. In another work in [23], Mao et al. propose a dual-polarized reconfigurable MIMO antenna using characteristic mode analysis. In this antenna, modal control and reconfigurable components are employed to attain efficient decoupling and polarization diversity. The antenna has low decoupling, is reconfigurable, and has stable radiation characteristics.

Following that in [24], He and Jin propose a compact microstrip MIMO antenna for sub-6 GHz 5G devices by considering radiator shaping and partial ground techniques. The proposed antenna has wide bandwidth, high isolation, and moderate gain.

Finally, in [25], Abdulkawi et al. propose a compact dual-band MIMO antenna for 5G and V2X communication devices. The proposed antenna design incorporates radiator shaping and ground plane techniques. The proposed antenna has good impedance matching, low coupling, and stable radiation characteristics.

3. PROPOSED SINGLE ANTENNA DESIGN AND OPTIMIZATION

In this section, the design methodology and optimization process for the proposed microstrip MIMO antenna for sub-6 GHz frequency band will be explained. The antenna configuration, geometry, and material properties will be described, and then the design evolution and optimization process for the antenna will be explained. The design evolution and optimization process for the antenna will be explained, with a focus on impedance matching, radiation efficiency, and reduction of mutual coupling, which are essential for a compact MIMO antenna for 5G technology in the sub-6 GHz frequency band.

3.1. Planar Microstrip Monopole Antenna (PMMA) Design

The proposed PMMA is inspired by a planar microstrip monopole structure on a dielectric substrate with a partial ground plane or defected ground structure, as indicated by the general structure of this antenna type presented in Figure 1. Planar monopole antennas are popularly used within sub-6 GHz wireless networks because of their small form factor, simple geometry, wide bandwidth operation, and suitability for printed circuit board technology. The proposed antenna is quite different from a microstrip patch antenna because it does not require a full ground plane to operate effectively; rather, it utilizes a partial ground plane to enable the operation of the radiating element as a quarter-wavelength resonator. The operation of this antenna is beneficial because it increases the fringing fields on the edges of the radiating element, which is a vital requirement of a compact sub-6 GHz antenna.

The antenna is designed on an FR4 substrate with a relative permittivity of (ε_r), thickness of the substrate (h), and loss tangent ($\tan\delta$). The selection of the substrate is a trade-off among cost, mechanical stability, and performance at sub-6 GHz frequencies. The metal layer is made of copper of thickness t, which is much smaller than the wavelength and hence does not affect the resonant properties of the structure. The effective dielectric constant of the structure is less than the substrate's

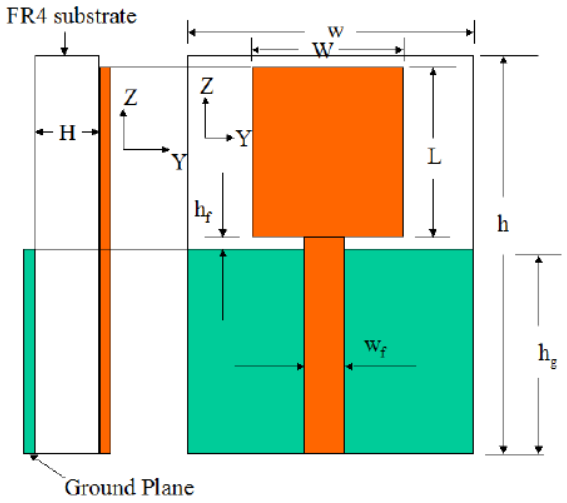

FIGURE 1. General configuration of a planar microstrip monopole antenna.

dielectric constant as a result of the fringing fields associated with the planar structure and partial ground plane. It can be approximated as given by the following equation [26]:

$$\varepsilon_{eff} = \frac{\varepsilon_r + 1}{2} + \frac{\varepsilon_r - 1}{2}\left(1 + 12\frac{h}{W_f}\right)^{-\frac{1}{2}} \tag{1}$$

where W_f refers to the width of the microstrip feeding line. This parameter plays a key role in determining the guided wavelength and the resonant frequency of the antenna. The parameter h refers to the height (thickness) of the antenna substrate.

For the case of the planar monopole antenna, the fundamental resonance occurs when the effective electrical length of the radiator is approximately one quarter of the guided wavelength. The guided wavelength λ_g is given by means of the following equation:

$$\lambda_g = \frac{c}{f_r\sqrt{\varepsilon_{eff}}} \tag{2}$$

where the parameter c is the speed of light in free space constant, and f_r is the desired resonant frequency.

Accordingly, due to the presence of the fringing effect concept in the microstrip antennas, the effective monopole length L_{eff} can be approximated as in the following equation:

$$L_{eff} \approx \frac{\lambda_g}{4} = \frac{c}{4f_r\sqrt{\varepsilon_{eff}}} \tag{3}$$

In the proposed antenna design, the effective length is formed by the combination of the main radiator length and the extended current paths introduced by comb-shaped strips. These extensions increase the electrical length without significantly increasing the physical size, enabling compact operation at the target sub-6 GHz frequency. In order to ensure the proper impedance matching between the antenna and excitation source, a 50-Ω microstrip feeding line is employed in this work. The width of the feed line W_f can be mathematically calculated by using the standard microstrip transmission line

TABLE 1. Preliminary antenna dimensions derived using MATLAB-based analytical calculations.

Parameter	W_s	L_s	h	W_p	L_p	W_g	L_g	W_f	L_f
Description	Antenna Substrate Width	Antenna Substrate Length	Antenna Substrate Height	Radiating Patch Width	Radiating Patch Length	Ground Plane Width	Ground Plane Length	Feed Line Width	Feed Line Length
Valu	25 mm	21 mm	1.6 mm	15.2 mm	11.3 mm	25 mm	6.4 mm	3.0 mm	6.4 mm

theory, as in the following equation: For $\frac{W_f}{h} \leq 2$:

$$Z_0 = \frac{60}{\sqrt{\varepsilon_{eff}}} \ln\left(\frac{8h}{W_f} + \frac{W_f}{4h}\right). \tag{4}$$

For $\frac{W_f}{h} > 2$:

$$Z_0 = \frac{120\pi}{\sqrt{\varepsilon_{eff}}\left(\frac{W_f}{h} + 1.393 + 0.667 \ln\left(\frac{W_f}{h} + 1.444\right)\right)}. \tag{5}$$

The partial ground plane is very significant for the impedance bandwidth and radiation performance of the planar monopole antenna. The truncation of the ground plane improves the current distribution and fringing fields, which enhance impedance matching and bandwidth performance. The length of the ground plane L_g is normally selected to be a fraction of the guided wavelength and is related by the following equation [27]:

$$L_g \approx (0.2 \sim 0.3)\, \lambda_g \tag{6}$$

It is necessary to mention that optimizing L_g directly affects the return loss and radiation efficiency of the antenna.

After implementing the design by employing the previously mentioned Equations (1)–(6) with a MATLAB-based computational code developed for antenna dimension calculations, the antenna design process is initiated by specifying the fundamental design parameters. These parameters include targeted resonant frequency (i.e., $f_r = 6$ GHz), relative permittivity corresponding to the FR4 substrate, substrate thickness $h = 1.6$ mm, copper metallization thickness of 0.035 mm, and input impedance $R_{in} = 50$. These initial values serve as the basis for the determining the physical dimensions of the proposed antenna and for guiding subsequent optimization steps.

Subsequently, after determining the dimensions of the antenna by implementing the MATLAB code, the next step in the design process involves creating a three-dimensional model of the antenna using Computer Simulation Technology (CST) software. The electromagnetic analysis of the antenna is performed by implementing the Finite Integration Technique (FIT), which allows for the accurate analysis of complex planar structures of the antenna. The geometric parameters determined by the MATLAB code are presented in Table 1.

After this step, the antenna structure is created according to the dimensions determined by the MATLAB code, as shown in Figure 2.

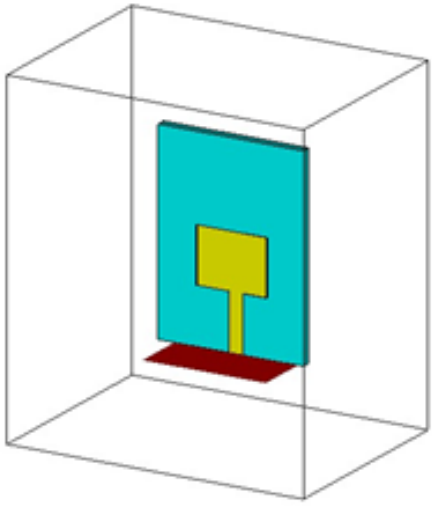

FIGURE 2. Simulated single monopole microstrip antenna in CST software.

3.2. Optimized PMMA Design

In this section, the optimization of the suggested planar microstrip monopole antenna design will be discussed in detail, considering a systematic parametric analysis approach. In this context, a parameter sweep approach, i.e., changing the parameters, is considered to examine the effects of significant geometrical parameters on the impedance matching, frequency band, and radiation characteristics of the planar microstrip monopole antenna design. In this context, stub elements are incorporated and appropriately varied to improve the current distribution, impedance matching, and electrical length of the planar microstrip monopole antenna design, thereby achieving the required sub-6 GHz frequency band characteristics.

Once the preliminary design phase was completed, the antenna's size was further refined through an iterative trial and error optimization process, which led to the desired impedance matching and radiation performance. The geometrical parameters were varied accordingly until the desired resonance and bandwidth characteristics were achieved.

The optimization process of the antenna began by adding two short stubs along the top edge of the radiating patch. The number of stubs was further increased from two to three and later to seven, all in an attempt to enhance the impedance matching properties of the antenna. All the stages leading up to the seven-stub version are shown in Figure 3.

The incorporation of these stubs has significant benefits in the electromagnetic design. The incorporation of the stub elements results in an increase in the effective electrical length of

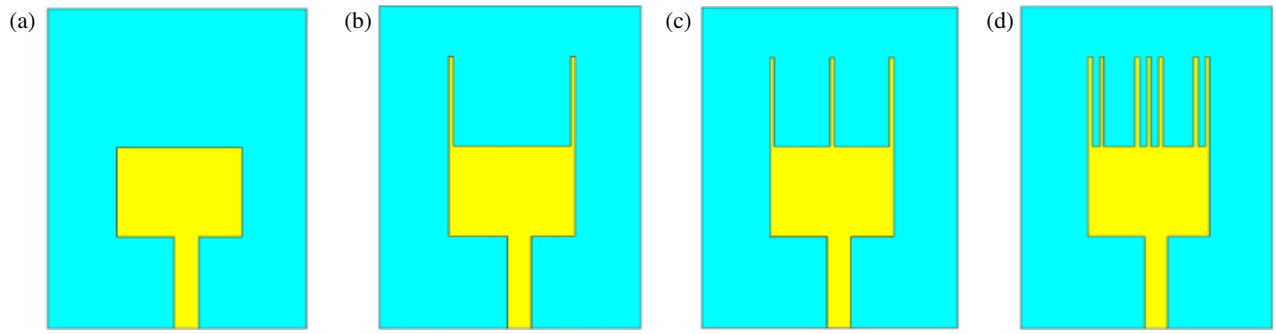

FIGURE 3. Design evolution steps of the proposed antenna enhancement. (a) Optimized PMMA. (b) Optimized PMMA with 2 stubs. (c) Optimized PMMA with 3 stubs. (d) Optimized PMMA with 7 stubs.

the radiator. This is done without an increase in the physical size of the antenna. It ensures the tuning of the resonant frequency while ensuring that the antenna is compact. The stub elements also have the effect of modifying the surface currents. The stub elements introduce multiple current paths along the radiating edge of the antenna. This ensures the excitation of multiple resonant modes. The coupling and interactions of these modes improve the bandwidth and the stability of the resonant modes. The distributed nature of the stub elements ensures smoother current flow. This results in improved impedance matching and reduced reflection loss.

After the evaluation of the seven-stub configuration, the number of stubs is increased to eleven. This increase in the number of stubs results in optimal performance. The optimized PMMA geometry with the increased number of stubs is provided in Figure 4.

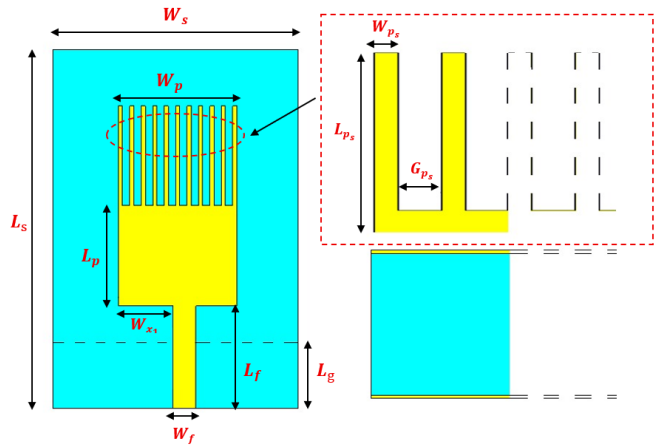

FIGURE 4. Proposed PMMA.

From the analysis of the reflection coefficient of the different configurations, it is evident that the increase in the number of stubs results in deeper resonance. Among the different configurations, the eleven-stub configuration has the lowest return loss. The optimized geometric parameters are provided in Table 2.

3.3. Optimized PMMA Fabrication

After the completion of the electromagnetic simulation and optimization process for the designed planar microstrip monopole antenna, the fabrication process for the optimized antenna was initiated. The final layout for the antenna was exported in the Gerber file format for the fabrication of the printed circuit board (PCB) for the antenna. The substrate used for the fabrication of the antenna was an FR-4 substrate with a thickness of 1.6 mm and a relative permittivity of 4.4, as chosen for the simulation model.

TABLE 2. Dimension illustration for the proposed PMMA.

Parameter	Size (mm)	Parameter	Size (mm)
W_s	24	L_g	6
L_s	35	W_f	2.23
h_s	1.6	L_f	10
W_p	11.6	W_{p_s}	0.4
L_p	9.8	L_{p_s}	9.
W_g	24	G_{p_s}	0.72
L_g	6	W_{x_1}	5.37

After the fabrication process, experimental validation was carried out in order to verify the results obtained through simulation. The antenna design was tested under a controlled environment by employing RF measurement equipment. The antenna design was tested inside an anechoic chamber, which is necessary for the accurate measurement of the antenn's radiation characteristics. The anechoic chamber is useful for minimizing the effects of external reflections. The reflection coefficient (S_{11}) was obtained by employing a calibrated vector network analyser (VNA). The antenna design and measurement setup are shown in Figure 5. The results obtained through the experiment were compared with those obtained through simulation in order to verify the accuracy of the antenna design.

3.4. Results and Analysis for the Proposed Single PMM

In this section, the simulated and measured results for the proposed design of the single planar microstrip monopole antenna (PMMA) are presented and discussed. For this antenna design, the antenna performance is analyzed in terms of reflection coefficient (S_{11}), gain, and radiation pattern to assess its applicability for sub-6 GHz frequency bands. Special emphasis is given to compare the results for the configurations without stubs and

TABLE 3. Summary of S_{11} performance for PMMA stub configurations.

Configuration	Main Resonant Frequency (GHz)	S_{11} (dB)	Bandwidth	Matching Quality
2 Stubs	≈ 6.0 GHz	≈ -15	Narrow	Moderate
3 Stubs	≈ 6.0 GHz	≈ -17	Slightly improved	Good
7 Stubs	≈ 6.0 GHz	≈ -19	Improved	Very Good
Optimized (Final Dimensions)	≈ 5.7–6.0 GH	≈ -11	Wide and stable	Acceptable but shallow resonance
Proposed (11 Stubs)	**≈ 6.0 GHz**	**≈ -20**	**Widest and most stable**	**Excellent (Best Performance)**

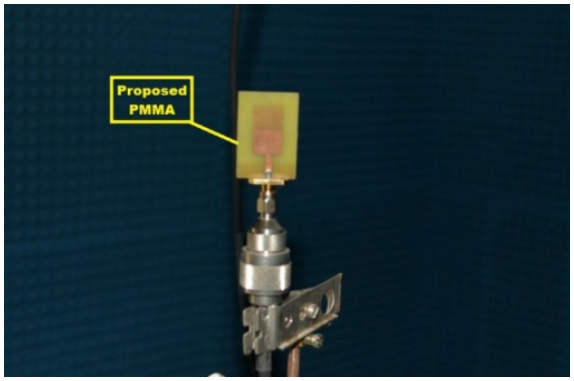

FIGURE 5. Photograph of the fabricated PMMA inside the anechoic chamber.

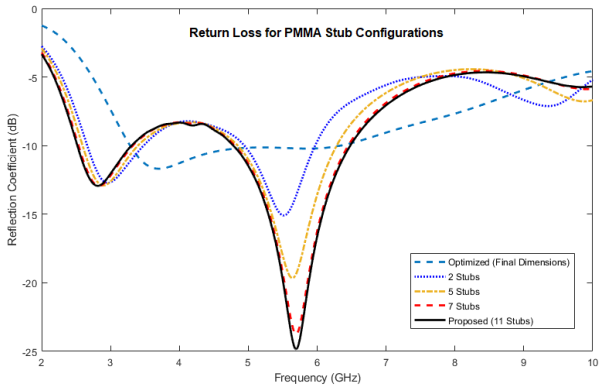

FIGURE 6. Simulated S_{11} for different stub configurations.

with eleven stubs to clearly show the effect of stubs on the antenna's electromagnetic characteristics. By studying these two configurations, the improvement in antenna matching and radiation characteristics using the optimization process can be easily identified. The comparison between simulated and measured results also validates the antenna design obtained from the optimization process.

3.4.1. PMMA Return Loss Results

The antenna return loss (S_{11}) is one of the fundamental parameters that are used to measure the amount of power reflected back from the antenna input port to the source of the power due to the impedance mismatch between the feed line and radiating element. The return loss is given in decibels (dB), and lower values indicate better impedance matching and efficient power transfer to free space. From Figure 6, the reflection coefficient for the PMMA stub configurations improves with the addition of stubs.

The reference PMMA configurations with 2 and 3 stubs presents moderate resonance characteristics with S_{11} values around -13 dB at 3 GHz frequency and a deeper resonance around 6 GHz with values between -15 dB and -17 dB. When the number of stubs is increased to 7, the resonance becomes sharper and deeper, showing better impedance matching characteristics. The proposed optimized design with 11 stubs shows the best results in terms of impedance matching characteristics with the lowest return loss around -20 dB at 6 GHz frequency, confirming better resonance and energy radiation characteristics. Furthermore, the optimized (final dimensions) design shows better impedance characteristics over a wide frequency band with values lower than -10 dB. A numerical summary of the results is given in Table 3.

This is due to the stub loading technique that improves the effective electrical length and surface currents on the patch to improve the energy radiation characteristics and resonance within the sub-6 GHz frequency band. Furthermore, the results show that the stub loading technique improves impedance matching characteristics using the geometrical optimization process for 5G sub-6 GHz frequency bands.

3.4.2. Antenna Efficiency

Antenna efficiency refers to the ability of the antenna structure to convert the power supplied to the antenna into electromagnetic waves effectively. It is usually determined by the radiation efficiency, which accounts for conductor and dielectric losses, and the total efficiency, which accounts for mismatch losses at the input port of the antenna structure. For a compact antenna designed for sub-6 GHz 5G communication, high efficiency over the frequency band of operation is critical for reliable communication and minimal power dissipation.

The simulated efficiency performance of the designed antenna is depicted in Figure 7. Note that the results were obtained using a full-wave electromagnetic simulator. This is because it is not easy to experimentally measure the radiation efficiency in the testing center due to different practical limitations. From the results depicted in Figure 7, it is evident that the radiation efficiency is above 0.8 over a wide frequency band. This indicates

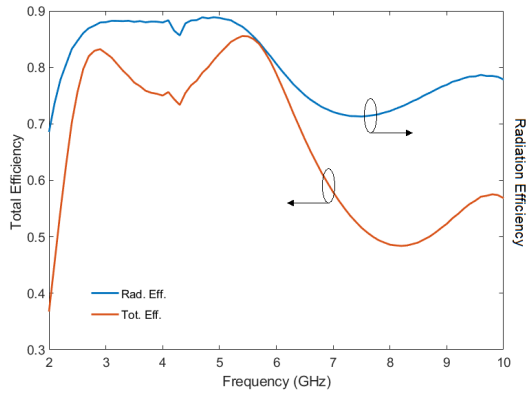

FIGURE 7. Efficiency of a proposed PMMA.

that the dielectric and ohmic losses are well controlled. Similarly, the total efficiency also behaves in a comparable manner and is above 0.7 over the major operating frequency band around the target frequency. This indicates that the impedance matching is effective and that the power transfer from the feed network to free space is efficient. Even though the total efficiency slightly drops at higher frequency values, the results show that the efficiency values over the intended 5G frequency band are stable and sufficient. This indicates that the optimized geometry and partial ground structure have been successful in maintaining high radiation efficiency while keeping the antenna compact in size.

3.5. PMMA MIMO Design

Once the design and validation of the suggested single PMMA were completed, the design of the 2×2 MIMO arrangement was carried out using the same optimized radiating element but this time placed on an FR4 substrate of a thickness of 1.6 mm with the same properties. Although the single element showed excellent performance in terms of impedance matching and radiation efficiency, there are additional electromagnetic issues that need to be considered when several radiating elements are integrated into a small area. In MIMO configurations, where several radiating elements are placed in a small area, coupling effects between adjacent radiating elements are of great importance. Surface-wave propagation and coupling effects between ports are also important issues. As a result, the impedance bandwidth and efficiency of the single PMMA need to be maintained in the multi-element MIMO arrangement to support reliable sub-6 GHz 5G operations.

In order to overcome these issues without adding complexity to the structure, the proposed design makes use of an orthogonal placement technique. As depicted in Figure 8(a), four identical PMMA components are placed symmetrically on a substrate of size $60 \times 60\,\text{mm}^2$, with adjacent components oriented by 90° with respect to one another. This ensures that the radiated electric fields of adjacent components are perpendicular to one another, thus providing polarization diversity and minimizing coupling effects. As depicted in Figure 8(b), the backside of the structure provides the ground plane and the feeding mechanism for balanced current distribution.

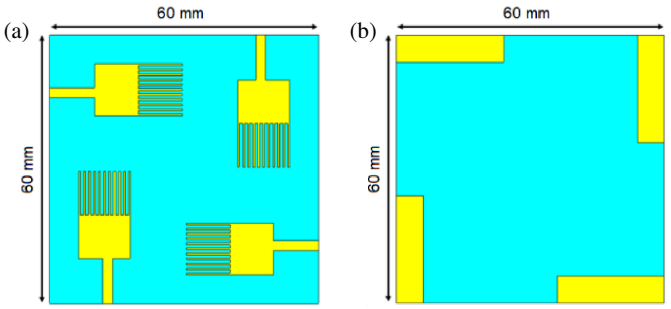

FIGURE 8. Simulated 2×2 MIMO design. (a) Front view. (b) Back view.

The fabricated prototype of the proposed 2×2 MIMO antenna design is shown in Figure 9. Both the front and rear views of the figure verify the compact integration of the proposed four radiating elements and their corresponding SMA connector types. The physical implementation of the proposed design resembles the simulated model. The single-element PMMA, which formed the basic building block of the proposed MIMO structure, was previously optimized using an iterative parametric analysis method. The final optimized element had a reflection coefficient of $S_{11} \approx -21.84\,\text{dB}$ at a frequency of 5.69 GHz, with an impedance bandwidth of 4.78 GHz to 6.98 GHz for $S_{11} \leq -10\,\text{dB}$. The optimization of the single-element structure was followed by simulation and experimental validation, after which the design was copied and configured to form the proposed four-port MIMO structure in an orthogonal configuration, thereby creating the proposed MIMO antenna design that is compact in size, stable in performance, and suitable for use in sub-6 GHz 5G wireless applications.

In order to validate the overall performance for the proposed fabricated PMMA MIMO antenna structure, the antenna was measured experimentally inside an anechoic chamber in the testing center, as exhibited in Figure 10. The measurement results are presented below, validating the accuracy of the design and fabrication process. The analysis of the measured and simulated results is presented in the following section, and they have a good agreement.

3.6. Results and Analysis for the Proposed MIMO PMM

In order to test the efficacy of the proposed orthogonal placement method, a comparative analysis was performed using two traditional 2×2 MIMO systems, namely Mirrored (Type 1) configuration and Front-to-Front (Type 2) configuration. The comparison criterion used was the reflection coefficient, S_{11}, which determines the impedance matching characteristics of each antenna port to its respective feed line. For the efficient operation of the antennas, a reflection coefficient of less than $-10\,\text{dB}$ is necessary to ensure that more than 90% of the power is transferred to the antenna and not reflected to the source [20].

The simulated results presented in Figure 11 clearly show that the orthogonal configuration has better performance than the other two conventional configurations. Although all three configurations have satisfied the $-10\,\text{dB}$ matching criterion within the 34.–6.8 GHz frequency band, the proposed antenna has a much deeper resonance at the centre frequency of 5.5 GHz

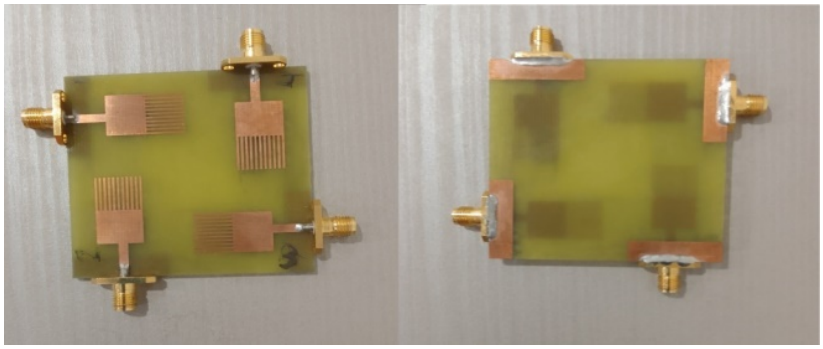

FIGURE 9. Fabricated 2×2 MIMO design.

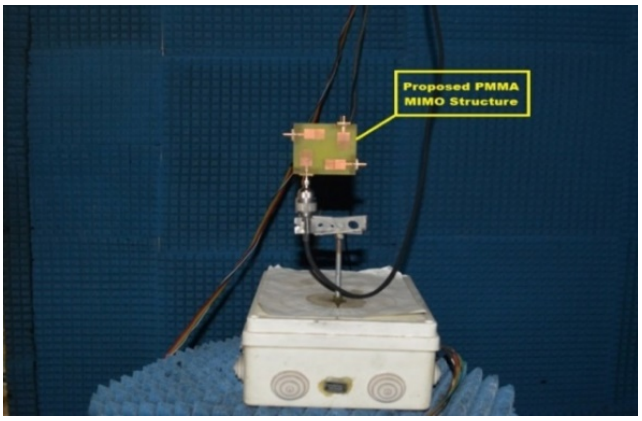

FIGURE 10. Photograph of the fabricated PMMA MIMO structure inside an anechoic chamber.

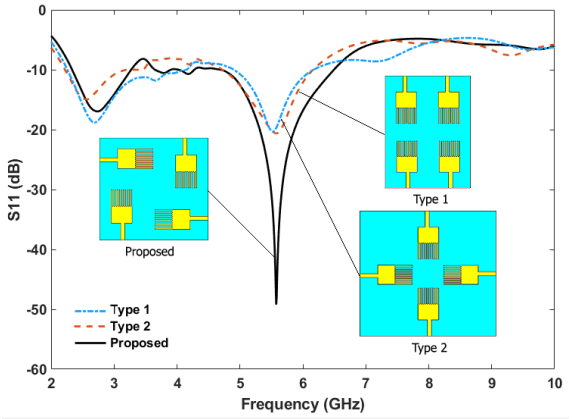

FIGURE 11. Simulated S_{11} comparison of the proposed PMMA MIMO configurations.

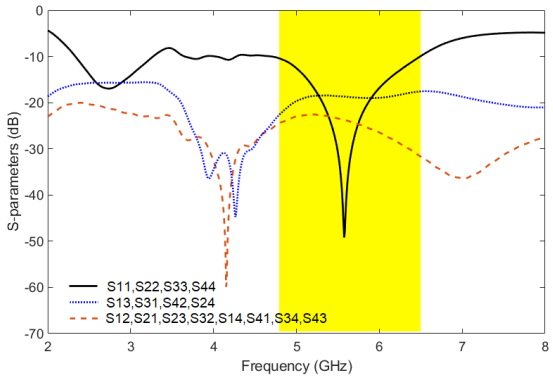

FIGURE 12. Simulated S-parameters of proposed PMMA MIMO configurations.

with an S_{11} value of around -49 dB. On the other hand, Mirrored (Type 1) and Front-to-Front (Type 2) configurations have shallow resonance at the same frequency with values around -19.75 dB and -19.56 dB, respectively.

This better performance of the proposed configuration may be mainly explained by the fact that the proposed configuration exhibits better decoupling between the elements due to the orthogonal orientation of the elements, which reduces the direct coupling between the elements by having the electric field polarization at right angles. It reduces the direct interaction between the elements and consequently increases the depth of resonance. In Type 1 and Type 2 configurations, the parallel orientation of the elements increases the direct interaction between the elements.

Hence, based on the above findings in Figure 11, the proposed orthogonal 2×2 MIMO structure is identified to offer the best impedance matching performance due to the lower reflection coefficient and better coupling suppression.

The simulated S-parameter results, as shown in Figure 12, reveal a strong level of symmetry in the structure, as well as good electromagnetic balance among the four radiating elements. In fact, the reflection coefficients S_{11}, S_{22}, S_{33}, and S_{44} display almost identical values over the entire frequency band, reflecting the uniformity of the impedance characteristics at all ports. In particular, at the center frequency of 5.5 GHz, there is a deep level of resonance for all ports, reaching a level of almost -49.5 dB.

Thus, the strong overlap of return loss curves confirms that the antenna elements have been properly designed and symmetrically positioned, ensuring uniform excitation conditions for all ports. This uniform behaviour of the antenna elements is very critical for MIMO systems, since nonuniform conditions between elements may increase correlation, thereby compromising diversity and radiation efficiency. In addition, the coupling parameters between ports, such as S_{12}, S_{13}, and S_{14}, have been well controlled, suggesting reduced interaction be-

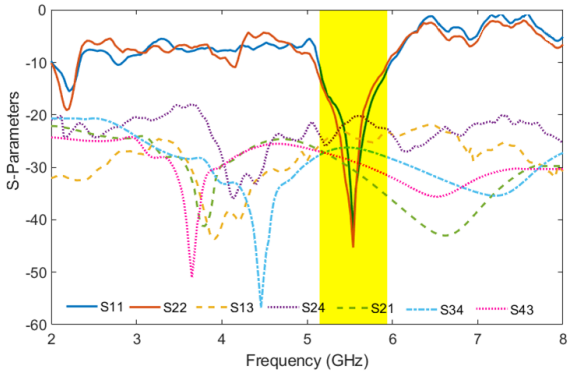

FIGURE 13. Measured mutual coupling parameters of the proposed PMMA MIMO configuration.

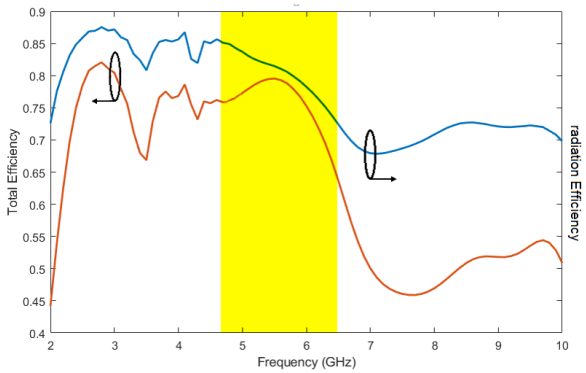

FIGURE 14. Simulated radiation and total efficiency of the proposed PMMA MIMO configuration.

tween ports for the highlighted sub-6 GHz operating band. The results obtained in the previous section have demonstrated the proposed 2×2 MIMO antenna configuration to have good and consistent impedance conditions, symmetry between ports, and reliable multi-port operation, thereby qualifying the antenna for sub-6 GHz 5G network operation.

The results obtained from the measurement of the designed 2×2 MIMO antenna in terms of S-parameters are depicted in Figure 13. From the measurement results, it is confirmed that the antenna has good impedance matching and isolation over the targeted sub-6 GHz frequency band. From the results obtained in this project, it is clear that the reflection coefficients (S_{11} and S_{22}) have good resonance near the centre frequency of 5.5 GHz. Even though there are some minor differences in the resonance frequency and magnitude, these differences are considered within the tolerance limits.

The discrepancies that are observed between the simulation and measurement results can be explained by the fact that there are certain factors associated with the fabrication process. These factors include the permittivity of the substrate, the slight variations in the thickness of the copper, and the slight imperfections that are associated with the soldering process. These factors can cause slight changes to the effective length of the antenna. In addition, the SMA connectors, feed lines, and losses that are associated with the connectors can cause slight mismatches between the ports. The measurement conditions can also cause the observed discrepancies. This is because the coaxial cables that are placed near the antenna can cause reflections.

With respect to isolation performance, the mutual coupling parameters (S_{21}, S_{34}, S_{43}, etc.) are found to be below -15 dB for the indicated operating region, which is considered satisfactory for a compact MIMO structure. At some frequency points, the isolation level is found to be above -50 dB, which indicates the presence of extremely low levels of coupling between the concerned port pairs. Though the isolation curves do not resemble each other perfectly, as expected under ideal simulation conditions, they do show a fair degree of symmetry with respect to the corresponding ports.

From the measured results, it has been observed that the data correlates well with the simulated data, and the robustness of the orthogonal configuration has also been validated, ensuring the antenna's functionality for a stable multi-port, sufficient isolation, and impedance characteristics for sub-6 GHz 5G MIMO technology.

The performance of the suggested 2×2 MIMO antenna structure in terms of efficiency is presented in Figure 14. Both the radiation efficiency and the total efficiency were considered for the evaluation. It is clearly shown that the fundamental radiation ability of the antenna is not influenced by the presence of the other elements. The radiation efficiency is still at a high level over the frequency band. This confirms the fact that the excessive coupling is properly mitigated by the structure, which maintains the fundamental radiation properties of the single element.

A small reduction in total efficiency is noted in the range of 3.33–3.54 GHz, in which the efficiency decreases slightly below 0.7. This reduction in efficiency is normally expected in compact MIMO systems. In this case, the elements in the antenna are closely spaced, and this results in some losses. As a result, some of the input power accepted by the antenna may not be radiated. This results in a small reduction in efficiency.

In spite of this small change, the antenna still exhibits a total efficiency of greater than 0.8 in the main operating band centered at the target sub-6 GHz frequency. This level of efficiency can be classified as very good for a compact multi-port MIMO antenna. Moreover, the total efficiency of the MIMO antenna configuration remains similar to the efficiency of the single-element antenna. This ensures that the radiation stability of the structure remains intact with minimal losses due to interaction between the antenna elements. In this way, the results verify the efficiency of the proposed antenna configuration for multi-element operation with minimal loss in efficiency.

The gain performance of the proposed 2×2 MIMO antenna is shown in Figure 15, in which the simulated and measured maximum gain values are plotted over the operating frequency range. It is observed that, at the centre frequency of 5.5 GHz, the simulated peak gain value is nearly 4.73 dBi, while the measured gain value is 4.70 dBi. The negligible difference between the two results indicates a good correlation between the simulated and experimental results, which validates the accuracy of the electromagnetic model and fabrication process.

Within the highlighted sub-6 GHz operating band, the antenna exhibits a gain level higher than 4 dBi. This can be considered appropriate for modern 5G wireless communication

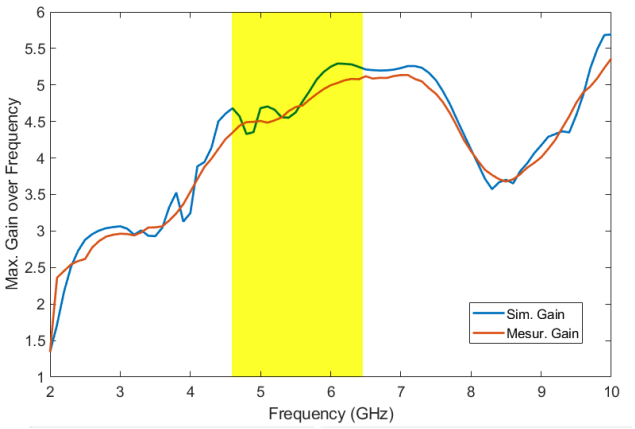

FIGURE 15. Simulated and measured maximum gains of the proposed PMMA MIMO configuration.

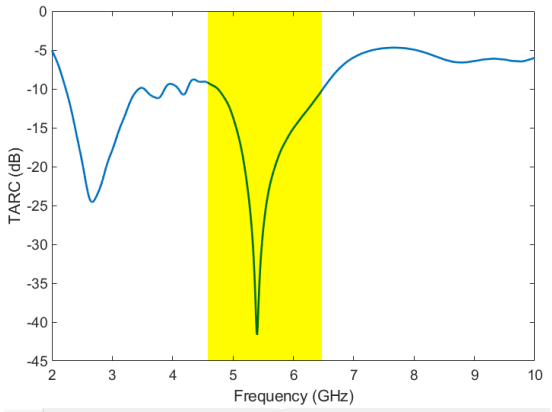

FIGURE 16. TARC of the proposed PMMA MIMO configuration.

systems [28]. The steady-state gain characteristic over the operating band signifies appropriate radiation efficiency and current distribution across the MIMO elements. Some fluctuations between the simulated and measured curves for other frequencies can be attributed to various implementation factors. The similarity between the simulated and measured curves for the antenna's gain characteristic signifies the robustness of the proposed orthogonal 2×2 MIMO concept. The gain level achieved by the proposed antenna signifies its suitability for sub-6 GHz 5G wireless communication systems.

Total Active Reflection Coefficient (TARC) is a key parameter for the performance evaluation of multi-port MIMO antennas. It is unlike other conventional reflection coefficients, such as S_{11} or S_{22}, which only evaluate the performance of each port individually under the condition of single-port excitation [29]. TARC considers the simultaneous excitation of multi-ports and also includes the effects of mutual coupling, active impedance variation, and phase considerations of the input signals.

One of the major benefits of using TARC is that it measures the total reflected power by exciting all ports simultaneously, rather than individually. This means that it is a complete measure of active matching performance, coupling suppression efficiency, and stability of a MIMO system. In a mathematical sense, TARC can be expressed mathematically as follows [30]:

$$\text{TARC} = \sqrt{\frac{\sum_{i=1}^{N}|b_i|^2}{\sum_{i=1}^{N}|a_i|^2}} \tag{7}$$

where a_i and b_i represent the incident and reflected wave amplitudes at the ith port, respectively, and N denotes the total number of antenna ports.

For a two-port antenna system with equal excitation applied to both the ports, the expression is simplified to

$$\text{TARC} = \frac{\sqrt{|b_1|^2+|b_2|^2}}{\sqrt{2}}. \tag{8}$$

This definition clearly shows how the TARC metric sums the total amount of combined reflected power from all the excited ports, making it a more suitable metric for assessing the active performance of MIMO antennas as opposed to traditional single-port reflection metrics.

The TARC response of the proposed antenna is depicted in Figure 16, where the active multi-port performance of the 2×2 MIMO antenna is assessed over the frequency band of operation. As shown, a deep minimum is observed around the centre frequency of about 5.5 GHz, where the TARC response is almost -42 dB. This shows that the active impedance matching is excellent, implying that most of the impinging waves are radiated with minimal reflection.

In the primary operating range, which lies between 3 and 6 GHz, the TARC remains below -10 dB. This ensures the efficient operation of the multi-port antenna in the desired range of frequencies. The values of TARC in this range show that the mutual coupling between the antenna ports and the phase interaction has been properly controlled to ensure the maintenance of active matching conditions.

At the extreme frequencies, particularly around 2 GHz and beyond 8 GHz, the TARC increases to around -5 dB. This indicates the reduced efficiency of the antenna in maintaining active matching conditions beyond the desired range. This is because of the impedance mismatch and reduced efficiency of the antenna at frequencies far removed from resonance. The results in Figure 16 show the strong efficiency of the proposed antenna in maintaining active conditions in the desired range of frequencies.

In the vicinity of the primary frequency of operation, which is 5.5 GHz, the antenna's active performance is excellent. At this frequency, the TARC curve dips to a deep minimum, which implies that a small amount of the input signal is reflected, and a greater amount of the signal is radiated. This shows that the antenna is efficient when all the ports are excited simultaneously. This is a requirement in MIMO systems. In addition, the low value of the TARC curve at this frequency shows that the coupling between the ports is well controlled, and the active impedance is stable. This shows that the MIMO performance of the antenna is stable, and the efficiency of the antenna is high. This frequency, therefore, can be said to be the best frequency of operation in the working band. Finally, the performance of the antenna is reliable and efficient, and this makes the antenna suitable for use in sub-6 GHz wireless communication systems.

The simulated diversity performance of the proposed MIMO antenna of 2×2 inside the CST environment is presented in Figure 17, where the Envelope Correlation Coefficient (ECC) and Diversity Gain (DG) are depicted. These parameters are of great importance for assessing the capacity of a MIMO system to offer independent paths and reduce the effect of multipath fading.

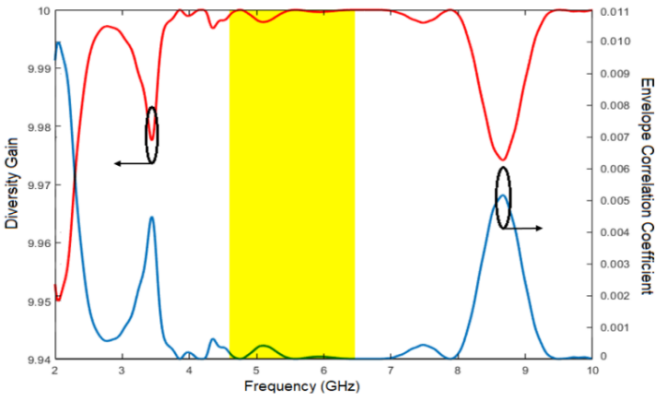

FIGURE 17. ECC and DG of the Proposed PMMA MIMO structure.

At the centre frequency of 5.5 GHz, the ECC remains extremely low, with values below 0.0001. Such extremely low correlation coefficient indicates that the radiation pattern of the antenna elements is highly uncorrelated. This simply implies that each of the ports contributes an independent signal component. This ensures that the MIMO system can exploit the spatial diversity to improve the link reliability and minimize the effects of fading.

Correspondingly, the diversity gain approaches 10 dB over the operating band, which is close to the maximum theoretical diversity gain for a well-functioning diversity system with two branches. This high DG clearly indicates that the antenna has the capability to ensure the robust diversity and communication links.

All-around, the very low ECC and high diversity gain values prove the effectiveness of the orthogonal placement strategy in minimizing the mutual correlation between ports. These results prove the suitability of the proposed antenna for advanced wireless communication systems operating in the sub-6 GHz band.

The results from the low ECC and high diversity gain values have further validated the efficiency and reliability for the proposed MIMO system in ensuring the good diversity for the antenna gain. For one, the correlation between the antenna ports is extremely low, ensuring that the elements are not coupled with one another. On the other hand, the diversity gain is close to ideal, ensuring that the antenna is not prone to multipath fading. These values have further validated the reliability and efficiency of the proposed MIMO system in ensuring that the signals remain consistent and that the degradation is minimal.

The simulated and measured far-field radiation patterns at 5.5 GHz are shown in Figure 18. The left column in this figure illustrates the radiation patterns in the E-plane ($\emptyset = 0°$), while the right column in this figure illustrates the radiation patterns in the H-plane ($\emptyset = 90°$) for all four ports.

In the E-plane, the main lobe levels at Ports 1 through 4 are similar and fall in the range of 17–18 dB(V/m), which indicates similar radiation levels for the antennas. The main beams' directions also lie between $160°$ and $180°$, which shows good structural symmetry and balanced current distribution. Small deviations in the beamwidth and the peak directions, such as the small deviation for Port 2 and the slightly wider pattern for Port 3, do not pose any problems.

In the H-plane, all ports show a similar radiation pattern, with the main-lobe levels ranging between 33 and 34 dB V/m and beam directions around $160°$. In terms of side-lobe levels, they are well controlled, ranging from -1.5 dB to -7 dB. This shows that there is minimal radiation in the side directions. In all ports, the patterns are identical, which shows that the excitation is balanced and that there is minimal pattern distortion. In terms of the E-plane and H-plane, they are identical, which shows that the structure is symmetric and that the use of the orthogonal placement technique does not affect the radiation pattern. They are important properties that are used to obtain MIMO performance.

Minor distortions in the radiation patterns may occur due to measurement results because of various limitations, such as alignment, connector, and environmental effects, in the measurement setup. However, if the main beam directions of the measurement results are close to the simulated results, and the magnitude of the radiation patterns is within acceptable limits, it can be concluded that the performance of the antenna is consistent and reliable. In this case, it can be concluded that the measurement results have good correlation with the simulated ones, thereby validating that the performance of the fabricated prototype is as expected.

Thus, a comprehensive comparison between the proposed MIMO structure and various designs reported in the literature is established to validate the performance improvements. Table 4 shows the competitive advantage of the proposed structure with respect to the size and performance. It is observed that the spacing between the radiating elements is relatively small; however, the antenna exhibits excellent performance with respect to impedance matching, isolation, and radiation properties. In conventional designs, the spacing between the radiating elements is relatively large to ensure effective mutual coupling reduction. However, the proposed structure is compact with effective mutual coupling reduction by appropriately arranging the radiating elements in an orthogonal manner.

Each of the microstrip ports for the proposed configuration manages the interference by being arranged at right angles relative to each other, making additional components for the separation of the signals redundant. Instead of slots, additional components are not required, like the earlier version of the MIMO antennas, where the unwanted signals are reduced by the way the device is shaped. By reducing the number of components, duplication becomes easier. Stability comes naturally if the configuration maintains a clean and simple look. By removing the need for additional insulator components, the device becomes easier to create. It performs well electrically, and yet it becomes cheaper to produce. It has been proven through the test, and the new version of the MIMO antenna maintains a

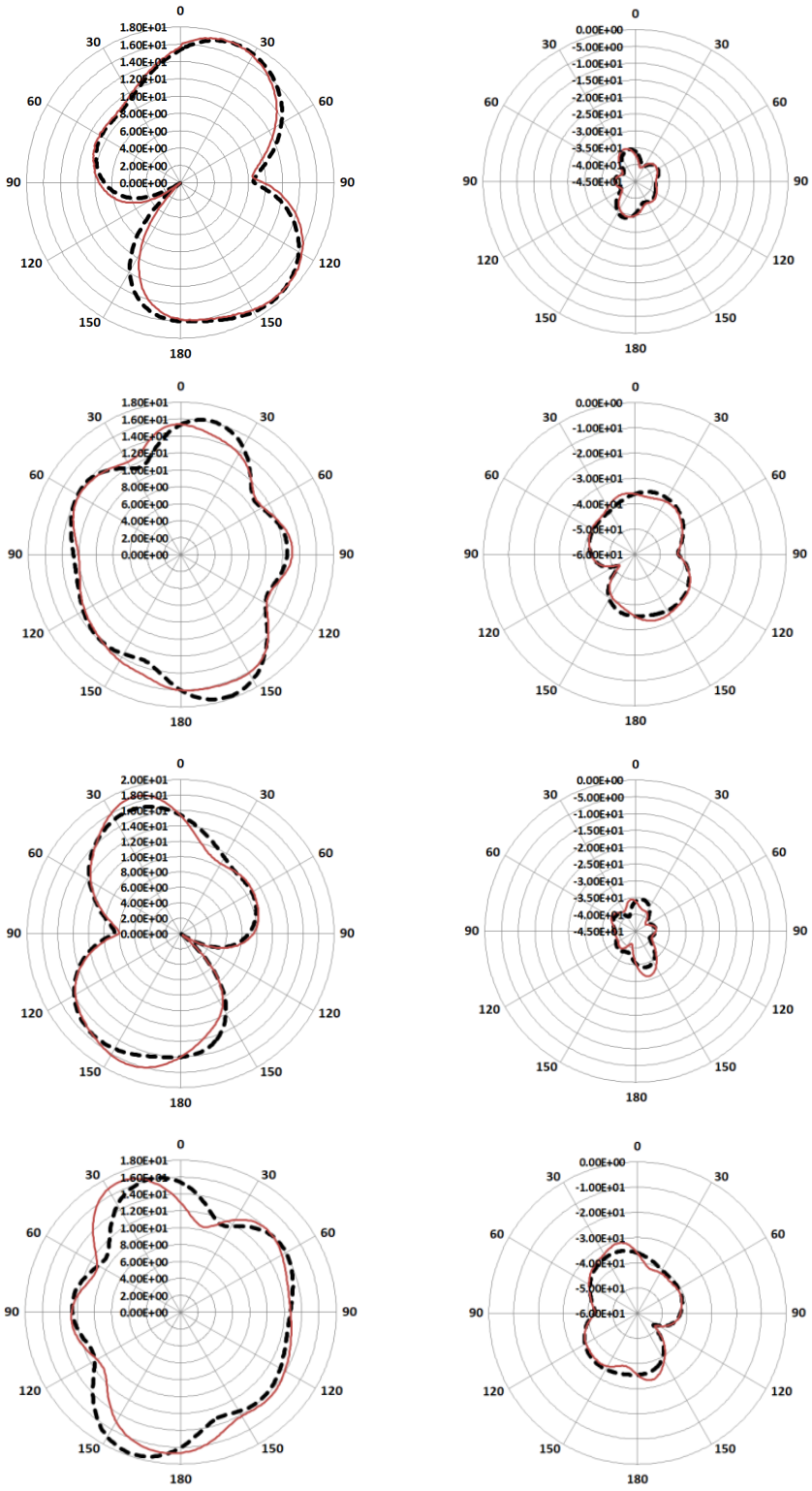

FIGURE 18. E-plane and H-plane radiation patterns at 5.5 GHz.

compact size of 60 mm by 60 mm. It performs well by matching the impedance and has radiation efficiency, yet the Envelope Correlation Coefficient is very low, at less than 0.0001, and the diversity performance is strong. These have been achieved without making any complicated changes, nor are layered configurations used, making the complexity under control while delivering the proper performance due to the simple configuration.

Unlike many of the older models discussed in the various studies, which often require more space and/or components to reduce interference, this new antenna is small yet works well and remains isolated. While some of the older models were

TABLE 4. Comparative performance analysis of published MIMO antennas.

Ref.	Year	Ports	Dimensions (mm^2)	S_{11} (dB)	BW (GHz)	Gain (dBi)	Efficiency	ECC
[20]	2023	4	90×90	-40	5.9/0.5	N/A	N/A	< 0.02
[21]	2023	8	105×60	-27	3.2–3.55	N/A	70	0.03
[23]	2023	4	180×180	-30	3.24/0.04	4.14	N/A	< 0.2
[24]	2022	8	51.2×51.2	-21	5.15–5.92	2.1	N/A	0.05
[31]	2021	4	60×70	-30	2.38–2.42	N/A	72	0.02
[32]	2023	4	64×64	-25	5.8/0.45	N/A	N/A	< 0.04
[33]	2023	4	60×60	-22.45	2.4/0.064	2.63	N/A	1.12×10^{-7}
[34]	2024	4	80×80	-44.4	5.9/0.17	6.3	N/A	0.02
[35]	2024	4	43×40	-15	4.97/0.32	1.2	$\eta_r = 0.8$	< 0.4
[36]	2020	8	136×68	-37	5.1–5.9	1.9	$\eta = 0.41$	< 0.1
[37]	2021	4	150×75	N/A	3.3–5.8	3.5–6	55–87	N/A
[38]	2022	4	150×75	-43	3.5–4.1	N/A	N/A	< 0.02
[39]	2021	2	160×70	N/A	5.6–5.67	N/A	N/A	< 0.005
[40]	2023	4	75×150	N/A	3.3–3.9	3	$\eta_r > 60$	< 0.001
Proposed	**2025**	**4**	$\mathbf{60 \times 60}$	$\mathbf{-49.22}$	**4.7–6.49**	**4.73**	$\boldsymbol{\eta_r = 0.81, \eta = 0.79}$	$\mathbf{< 0.0001}$

effective in boosting one feature, such as signal strength or isolation, they were larger, less efficient in other areas, and/or had lower error correlation numbers. On the other hand, this new MIMO antenna works well throughout the full range of below 6 GHz without wavering. From all directions, the findings suggest that this new MIMO antenna is a winner in terms of small size, good performance, and ease of design. This small antenna is efficient, keeps signals separate, and works well with data streams, making it a winner for today's sub-6 GHz world of 5G. What is impressive is how well everything fits together without compromising performance. In this case, simplicity does not mean compromise. Instead, it means that the structure works behind the scenes to provide gains. Each piece of this design works well. Not flashy, but gets the job done.

4. CONCLUSION

This paper has presented the design, fabrication, and experimental validation of a compact 2×2 orthogonal microstrip MIMO antenna for sub-6 GHz 5G applications. The proposed antenna occupies a limited footprint of $60 \times 60\,mm^2$ on an FR4 substrate and was developed to achieve high efficiency, strong isolation, and low inter-element correlation without introducing structural complexity. The design process began with the optimization of a planar microstrip monopole antenna (PMMA) using a systematic stub-loading technique and a partial ground structure to enhance impedance matching and radiation characteristics. The optimized element was then arranged in an orthogonal configuration to exploit polarization diversity as a natural mechanism for mutual coupling reduction. Unlike many conventional approaches that rely on decoupling networks, parasitic elements, metasurfaces, or multilayer structures, the proposed design achieves effective isolation through geometric arrangement alone, maintaining simplicity and cost-effectiveness. Both simulated and measured results demonstrate excellent performance. The antenna achieves a measured reflection coefficient of approximately $-49\,dB$ at 5.5 GHz, with a wide operating bandwidth from 4.7 to 6.49 GHz. High radiations and total efficiencies are maintained across the main band, and the measured peak gain reaches 4.70 dBi. The diversity performance is particularly notable, with an extremely low envelope correlation coefficient ($ECC < 0.0001$) and a diversity gain close to 10 dB, confirming strong spatial diversity and reliable multipath behaviour. Additionally, the TARC remains below $-10\,dB$ within the primary operating region, validating stable active multi-port performance. Finally, the proposed antenna provides a balanced combination of compact size, high efficiency, low correlation, and structural simplicity. The results confirm its suitability for integration into modern sub-6 GHz 5G wireless systems and highlight the effectiveness of orthogonal element placement as a practical and scalable solution for compact MIMO antenna design.

REFERENCES

[1] Shaik, R. B., P. Nagaradjane, I. Ioannou, V. Sittakul, V. Vasiliou, and A. Pitsillides, "AI/ML-aided capacity maximization strategies for URLLC in 5G/6G wireless systems: A survey," *Computer Networks*, Vol. 249, 110506, 2024.

[2] Aarti, S., S. Gowroju, and S. I. Ansarullah, "A comprehensive review of developments and challenges in the 6G internet of things," *Discover Networks*, Vol. 1, No. 1, 13, 2025.

[3] Akbar, M. S., Z. Hussain, M. Ikram, Q. Z. Sheng, and S. C. Mukhopadhyay, "On challenges of sixth-generation (6G) wireless networks: A comprehensive survey of requirements, applications, and security issues," *Journal of Network and Computer Applications*, Vol. 233, 104040, 2025.

[4] Md. Yunus, N. A., Z. M. Hanapi, S. Kamarudin, A. R. B. M. Sufian, F. M. Ali, N. Ripin, and H. Sofian, "Exploring the landscape of 6G wireless communication technology: A review," *International Journal of Advanced Computer Science & Applications*, Vol. 16, No. 5, 2025.

[5] Asif, S., *5G Mobile Communications Concepts and Technologies*, 1st ed., CRC Press, 2019.

[6] Osseiran, A. and J. F. M. P. Marsch, *5G Mobile and Wireless Communications Technology*, Cambridge University Press, 2016.

[7] Behera, B. R., H. Paik, J. A. Kumar, M. H. Alsharif, S. Saeed, and K. Yahya, "Implementation of smart metasurfaces for the sub-6 GHz 5G wireless systems: Design, optimization, and its synthesis for enhancing antenna's performance," *Scientific Reports*, Vol. 16, 10420, 2026.

[8] Albaihani, Y., R. Akram, E. A. Hajlaoui, A. M. Almohaimeed, Z. M. Almohaimeed, and A. Albaihani, "5.8 GHz microstrip patch antennas for wireless power transfer: A comprehensive review of design, optimization, applications, and future trends," *Electronics*, Vol. 15, No. 2, 311, 2026.

[9] Arnaoutoglou, D. G., T. M. Empliouk, T. N. F. Kaifas, M. T. Chryssomallis, and G. Kyriacou, "A review of multifunctional antenna designs for internet of things," *Electronics*, Vol. 13, No. 16, 3200, 2024.

[10] Yadav, S. V., M. V. Yadav, S. Raghavendra, and V. Gupta, "Next-generation compact antenna for robust defense and CubeSat communication," *Scientific Reports*, Vol. 16, 7596, 2026.

[11] Sultana, M., S. M. A. Z. Chowdhury, and M. A. Alim, "Compact U-slot microstrip antenna for Wi-Fi 5/6: Enhancing gain, bandwidth, and efficiency," *Journal on Wireless Communications and Networking*, Vol. 2026, 9, 2026.

[12] Shandilya, S., K. Gautam, G. Mathur, S. Jain, and D. K. Somwanshi, "A microstrip patch antenna with rectangular slots and parasitic elements," *Intelligent Systems Using Semiconductors for Robotics and IoT*, 183–190, CRC Press, 2026.

[13] Azzouz, A., R. Bouhmidi, M. E. Munir, M. M. Nasralla, and M. Chetioui, "Characterization and analysis of hybrid fractal antennas for multiband communication and radar applications," *Fractal and Fractional*, Vol. 10, No. 1, 47, 2026.

[14] Gayathri, R., K. Kavitha, D. R. Kumar, and P. Sundaravadivel, "Miniaturized dual-band MIMO antenna with high gain and isolation for mm-Wave applications," *Scientific Reports*, Vol. 16, 7402, 2026.

[15] Islam, T., F. Alsaleem, F. N. Alsunaydih, and K. Alhassoon, "Mutual coupling reduction in compact MIMO antenna operating on 28 GHz by using novel decoupling structure," *Micromachines*, Vol. 14, No. 11, 2065, 2023.

[16] Abdollahvand, M., G. R. Dadashzadeh, H. Ebrahimian, and M. Ojaroudi, "Compact ultra-wideband printed monopole antenna having frequency band-notch characteristic using defected ground structure," *Microwave and Optical Technology Letters*, Vol. 53, No. 10, 2363–2368, 2011.

[17] 3rd Generation Partnership Project (3GPP), "NR; User equipment (UE) radio transmission and reception; Part 1: Range 1 standalone," Technical Specification (TS) 38.101-1, Release 16, 2020.

[18] Saeidi, T., A. J. A. Al-Gburi, and S. Karamzadeh, "A miniaturized full-ground dual-band MIMO spiral button wearable antenna for 5G and sub-6 GHz communications," *Sensors*, Vol. 23, No. 4, 1997, 2023.

[19] Upadhyaya, T., I. Park, R. Pandey, U. Patel, K. Pandya, A. Desai, J. Pabari, G. Byun, and Y. Kosta, "Aperture-fed quad-port dual-band dielectric resonator-MIMO antenna for sub-6 GHz 5G and WLAN application," *International Journal of Antennas and Propagation*, Vol. 2022, No. 1, 4136347, 2022.

[20] Ez-Zaki, F., H. Belahrach, A. Ghammaz, S. Ahmad, A. Khabba, K. A. Belaid, A. Ghaffar, and M. I. Hussein, "Double negative (DNG) metamaterial-based Koch fractal MIMO antenna design for sub-6-GHz V2X communication," *IEEE Access*, Vol. 11, 77 620–77 635, 2023.

[21] Morsy, M. M., "Compact eight-element MIMO antenna array for sub 6 GHz mobile applications," *SN Applied Sciences*, Vol. 5, No. 10, 261, 2023.

[22] Hasan, M. M., M. T. Islam, M. Samsuzzaman, M. H. Baharuddin, M. S. Soliman, A. Alzamil, I. I. M. A. Sulayman, and M. S. Islam, "Gain and isolation enhancement of a wideband MIMO antenna using metasurface for 5G sub-6 GHz communication systems," *Scientific Reports*, Vol. 12, No. 1, 9433, 2022.

[23] Mao, X., Z. Zhang, and J. Wang, "Dual-polarized reconfigurable MIMO decoupled antenna design using characteristic mode analysis," in *2023 IEEE MTT-S International Microwave Workshop Series on Advanced Materials and Processes for RF and THz Applications (IMWS-AMP)*, 1–3, Chengdu, China, 2023.

[24] He, Z. and J. Jin, "Compact quad-port MIMO antenna with ultra-wideband and high isolation," *Electronics*, Vol. 11, No. 20, 3408, 2022.

[25] Abdulkawi, W. M., W. A. Malik, S. U. Rehman, A. Aziz, A. F. A. Sheta, and M. A. Alkanhal, "Design of a compact dual-band mimo antenna system with high-diversity gain performance in both frequency bands," *Micromachines*, Vol. 12, No. 4, 383, 2021.

[26] Pozar, D. M., *Microwave Engineering*, John Wiley & Sons, 2011.

[27] Abdollahvand, M., Y. Zehforoosh, B. Marufi, P. E. Kaleybar, and A. Dastranj, "A novel UWB in-body printed microstrip feed monopole antenna with dual band-stop capabilities," *Microwave and Optical Technology Letters*, Vol. 66, No. 9, e34317, 2024.

[28] Abdollahvand, M. and G. R. Dadashzadeh, "Compact double-fed dual annular ring printed monopole antenna for UWB application," *Journal of Electromagnetic Waves and Applications*, Vol. 23, No. 14–15, 1969–1980, 2009.

[29] Abdollahvand, M., B. A. Arand, K. Katoch, and S. Ghosh, "A novel and compact ultra-wideband printed monopole antenna with enhanced bandwidth and dual-band stop properties," *Microwave and Optical Technology Letters*, Vol. 66, No. 1, e33990, 2024.

[30] Sharma, M., B. R. Perli, G. Singla, T. Addepalli, S. Medasani, B. S. Sridevi, and T. Ali, "Micromachined mmWave 28.0/38.0 GHz MIMO antenna loaded with frequency selective surface for gain enhancement and SAR analysis for future wireless applications," *PLOS One*, Vol. 21, No. 2, e0342022, 2026.

[31] Li, M. and S. Cheung, "A novel calculation-based parasitic decoupling technique for increasing isolation in multiple-element MIMO antenna arrays," *IEEE Transactions on Vehicular Technology*, Vol. 70, No. 1, 446–458, Jan. 2021.

[32] Lamri, I. E. and A. Mansoul, "Design of CPW-fed dual-band four-element MIMO microstrip patch antenna for WLAN/WiMAX applications," in *2023 International Microwave and Antenna Symposium (IMAS)*, 83–86, Cairo, Egypt, Feb. 2023.

[33] Kikan, V., A. Dagar, S. Singh, S. Singh, N. C. Deo, A. Kumar, and M. Sharma, "A four-port novel inset-fed, rectangular MIMO-antenna designed for 2.40 GHz Bluetooth & Wi-Fi applications," in *2023 Second International Conference on Electrical, Electronics, Information and Communication Technologies (ICEEICT)*, 1–6, Trichirappalli, India, 2023.

[34] Pal, A. and V. S. Tripathi, "Quad-element MIMO antenna with diverse radiation pattern characteristics and enhanced gain for 5.9 GHz V2X communications," *AEU — International Journal of Electronics and Communications*, Vol. 176, 155119, 2024.

[35] Kumar, A., Neeraj, V. Prakash, and S. C. Padhy, "Four port MIMO antenna for IoT applications in public safety band and sub-6 GHz TDD 5G band," *Engineering Research Express*, Vol. 6, No. 1, 015039, 2024.

[36] Sim, C.-Y.-D., H.-Y. Liu, and C.-J. Huang, "Wideband MIMO antenna array design for future mobile devices operating in the 5G NR frequency bands n77/n78/n79 and LTE band 46," *IEEE Antennas and Wireless Propagation Letters*, Vol. 19, No. 1, 74–78, Jan. 2020.

[37] Zheng, Z., J. D. Ntawangaheza, and L. Sun, "Wideband MIMO antenna system for sub-6 GHz cell phone," in *2021 International Conference on Electronics, Circuits and Information Engineering (ECIE)*, 1–5, Zhengzhou, China, 2021.

[38] Alnahwi, F. M., Y. I. A. Al-Yasir, C. H. See, and R. A. Abd-Alhameed, "Single-element and MIMO circularly polarized microstrip antennas with negligible back radiation for 5G mid-band handsets," *Sensors*, Vol. 22, No. 8, 3067, 2022.

[39] Khan, J., S. Ullah, F. A. Tahir, F. Tubbal, and R. Raad, "A sub-6 GHz MIMO antenna array for 5G wireless terminals," *Electronics*, Vol. 10, No. 24, 3062, 2021.

[40] Parchin, N. O., Y. I. A. Al-Yasir, H. J. Basherlou, R. A. Abd-Alhameed, and J. M. Noras, "Orthogonally dual-polarised MIMO antenna array with pattern diversity for use in 5G smartphones," *IET Microwaves, Antennas & Propagation*, Vol. 14, No. 6, 457–467, 2020.